Supporting Information

Chemical and materials

All reagents were used as received. Sodium chloropalladate (Na_2PdCl_4), copper(II) chloride dihydrate ($CuCl_2 \cdot 2H_2O$), indium acetylacetonate ($In(acac)_3$), tungsten hexacarbonyl ($W(CO)_6$), *N*,*N*-dimethylformamide (DMF), glacial acetic acid, sodium citrate dihydrate, sodium hypochlorite (NaClO), sodium hydroxide (NaOH), potassium nitrate (KNO_3), potassium bicarbonate ($KHCO_3$), potassium sulfate (K_2SO_4), salicylic acid, N-(1-naphthyl)ethylenediamine dihydrochloride, ferric chloride ($FeCl_3$), phosphoric acid (≥85%), sulfanilamide, diacetyl monoxime (DAMO), and Nafion solution (0.5 wt%) were purchased from Aladdin Chemistry Co., Ltd. Thiosemicarbazide (TSC) and sodium nitroferricyanide were obtained from Shanghai Macklin Biochemical Co., Ltd.

In-situ attenuated total reflection Fourier transform infrared (ATR-FTIR) spectroscopy measurement. In-situ ATR-FTIR spectra were acquired on a Nicolet iS50 spectrometer equipped with a liquid nitrogen-cooled MCT detector, covering the spectral range of 1000–4000 cm^{-1}. A gold-coated silicon prism served as both the working electrode substrate and the infrared-reflective element. The catalyst was deposited onto this surface to form a thin film. A standard three-electrode configuration was employed, using an Ag/AgCl electrode (3 M KCl) and a Pt sheet as the reference and counter electrodes, respectively. Prior to each measurement, a background spectrum was collected at open-circuit potential. All spectra were recorded in CO_2-saturated 0.1 M KNO_3 and 0.1 M $KHCO_3$ solution electrolyte after a 15-minute stabilization at each applied potential, which was varied from –0.1 to –0.5 V vs. RHE.

Product analysis

Determination of gaseous products. The gaseous products (H_2 and CO) were analyzed using a gas chromatograph (Shimadzu GC-2014) equipped with both a thermal conductivity detector (TCD) and a flame ionization detector (FID), employing high-purity argon (99.999%) as the carrier gas. Quantification was performed by comparing the chromatographic peak areas against calibration curves established with certified standard gases.

Determination of urea, ammonia and nitrite. Determination of urea, ammonia and nitrite concentrations in the electrolyte after electrocatalysis was performed using established spectrophotometric methods: urea by the diacetyl monoxime method, ammonia by the indophenol blue method, and nitrite by the Griess method.[1] The procedures are detailed below.

Determination of urea. The concentration of as-produced urea was determined using the diacetyl monoxime method with spectrophotometry. First, an aliquot of post-reaction electrolyte was first diluted threefold to fit the linear range of the standard curve. Next, 1 mL of the diluted sample was mixed with 2 mL of an acid-ferric solution (prepared from 600 mL deionized water, 100 mL concentrated phosphoric acid, 300 mL concentrated sulfuric acid, and 100 mg ferric chloride) and 1 mL of a chromogenic reagent containing diacetyl monoxime (DAMO) and thiosemicarbazide (TSC) (0.5 g DAMO and 10 mg TSC dissolved and diluted to 100 mL with deionized water). The mixture was then heated at 110 °C for 15 min. After cooling to room temperature, its absorbance was measured at 525 nm using a UV-vis spectrophotometer. A calibration curve was established by applying the same procedure to a series of standard urea solutions prepared in the background electrolyte (Fig. S6), from which

the urea concentration in the sample was determined.

Determination of ammonia. The concentration of ammonia (NH_3) was quantified using the indophenol blue method with spectrophotometry. Three color reagents were prepared in advance: reagent A (1 M NaOH containing 5 wt% salicylic acid and 5 wt% sodium citrate), reagent B (0.05 M NaClO), and reagent C (1 wt% sodium nitroferricyanide, $C_5FeN_6Na_2O$). For analysis, 2 mL of the sample electrolyte was mixed sequentially with 2 mL of reagent A, 1 mL of reagent B, and 0.2 mL of reagent C. After thorough mixing, the solution was kept at room temperature for 2 h in the dark to allow complete color development. The absorbance was then measured at 655 nm using a UV-vis spectrophotometer. A calibration curve (Fig. S7) was constructed under identical conditions using a series of ammonium sulfate standards dissolved in the same background electrolyte, from which the ammonia concentration was determined.

Determination of nitrite. The nitrite content was determined via the Griess method. First, a chromogenic reagent was prepared by dissolving 0.4 g of sulfanilamide and 0.02 g of N-(1-naphthyl) ethylenediamine dihydrochloride in a mixture of 1 mL phosphoric acid and 5 mL deionized water. Subsequently, 5 mL of diluted catholyte was combined with 0.1 mL of the prepared reagent. Following a 20 min reaction at room temperature, the absorbance at 540 nm was recorded by UV-Vis. The concentration-absorbance curves were calibrated using a series of standard KNO_2 solutions with the same electrolyte concentrations used in the electrocatalysis experiments by the same processes (Fig. S8).

Calculation of yield and Faradaic efficiency

The calculation equations are as follows:

$$FE_{urea} = \frac{z \times C_{urea} \times V_{aq} \times F}{Q} \times 100\% \quad (1)$$

$$FE_{NH_3} = \frac{z \times C_{NH_3} \times V_{aq} \times F}{Q} \times 100\% \quad (2)$$

$$FE_{NO_2^-} = \frac{z \times C_{NO_2^-} \times V_{aq} \times F}{Q} \times 100\% \quad (3)$$

$$FE_{CO} = \frac{z \times n_{CO} \times F}{Q} \times 100\% \quad (4)$$

$$FE_{H_2} = \frac{z \times n_{H_2} \times F}{Q} \times 100\% \quad (5)$$

$$Yield_{urea} = \frac{C_{urea} \times V_{aq}}{t \times m} \quad (6)$$

where z denotes the number of electrons transferred, C_{urea} is the concentration of urea (mol L^{-1}), V_{aq} denotes the volume of electrolyte (V_{aq} = 30 mL), F is Faraday constant (96485 C mol^{-1}), C_{NH_3} is the concentration of NH_3 (mol L^{-1}), $C_{NO_2^-}$ is the concentration of NO_3^- (mol L^{-1}), n_{CO} denotes the amount of CO (mol), n_{H_2} denotes the amount of H_2 (mol), Q is the total charge amount, t denotes the time of electrolysis, and m denotes the mass of the loaded catalyst.

DFT calculation details. DFT calculations were performed utilizing the Vienna Ab Initio Simulation Package (VASP) with projector augmented wave (PAW) potentials and a plane-wave cutoff set at 520 eV.[2, 3] The generalized gradient approximation (GGA) with the Perdew–Burke–Ernzerhof (PBE) functional was employed to describe the exchange-correlation effects, supplemented by Grimme's semiempirical DFT-D3 method to incorporate van der Waals (vdW) interactions.[4] Structural optimizations were carried out with convergence thresholds of 10^{-5} eV for energy and 0.02 eV·Å-1 for forces. Both Indium-Inserted PdCu (110) and PdCu alloy (111) surfaces were optimized, employing a vacuum layer of 16 Å in all slab models to prevent interactions between periodic images and adsorbates. The adsorption energy (E_{ads}) for urea electrosynthesis was calculated as $E_{ads} = E_{Total} - E_{surf} - E_{adsorbate}$, where E_{Total} is the total energy of the adsorbate-surface system, E_{surf} is the energy of the pristine surface, and $E_{adsorbate}$ is the energy of the isolated molecule in a cubic periodic box. Post-processing of the computational data was conducted using the VASPKIT softwar,[5] while visualization of crystal structures and charge density distributions was carried out with the VESTA progra.[6]

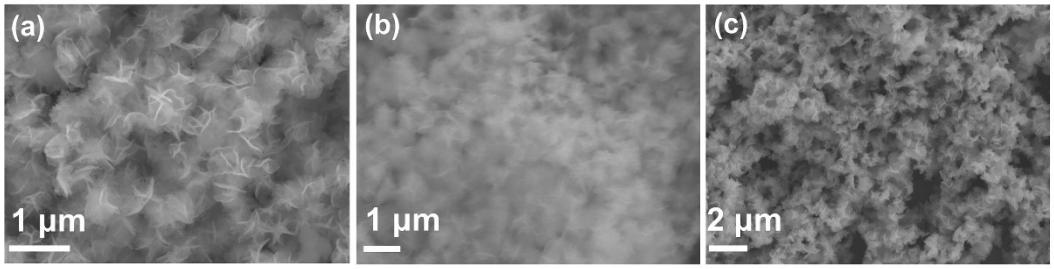

Fig. S1 SEM images of different PdCuIn metallene samples obtained by varying the reaction temperature and reaction times: (a) 160 °C, 12 h; (b) 220 °C, 12 h; (c) 240 °C, 36 h.

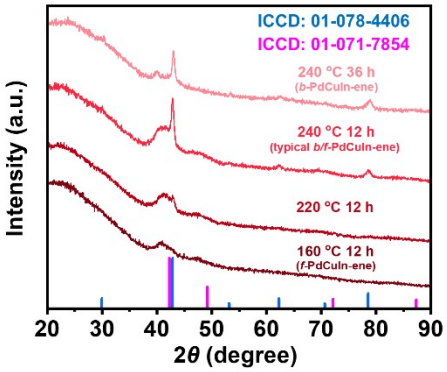

Fig. S2 XRD patterns of different PdCuIn metallene samples obtained by varying the reaction temperature and reaction times.

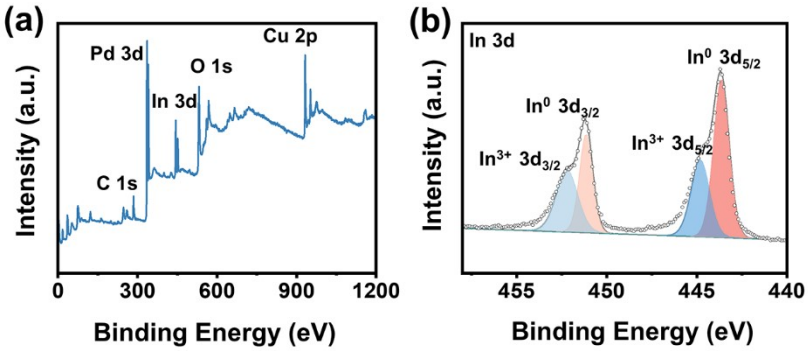

Fig. S3 (a) XPS survey spectrum and (b) high-resolution In 3d XPS spectrum of the *b*/*f*-PdCuIn-ene.

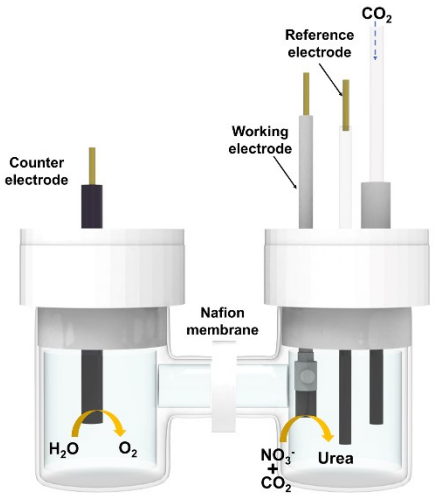

Fig. S4 Scheme of the three-electrode system in an H-type electrolytic cell for urea electrosynthesis.

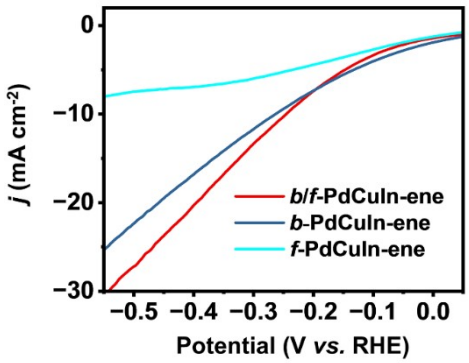

Fig. S5 LSV curves of various catalysts for co-electroreduction of NO_3^- and CO_2.

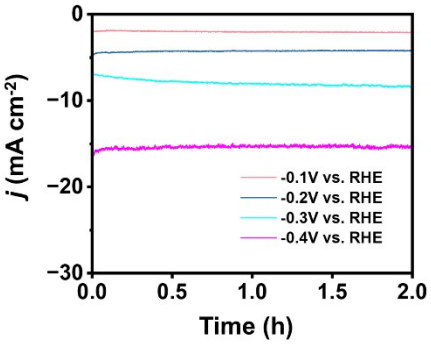

Fig. S6 Chronoamperometric (i-t) curves of the *b*/*f*-PdCuIn-ene for co-reduction of CO_2 and NO_3- under different applied potentials.

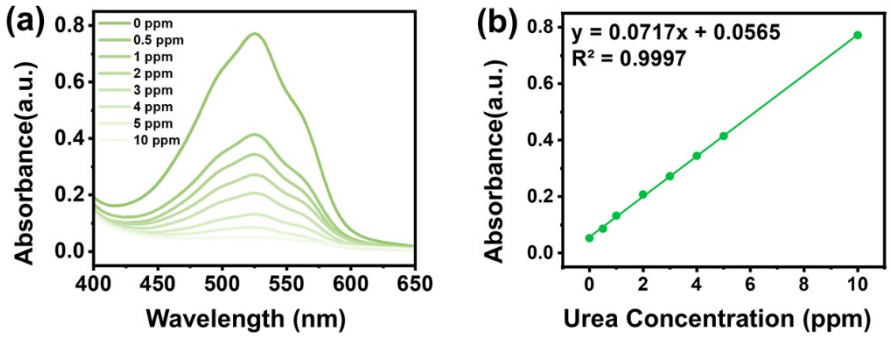

Fig. S7 (a) UV-Vis curves for different urea concentrations. (b) Calibration curve for urea.

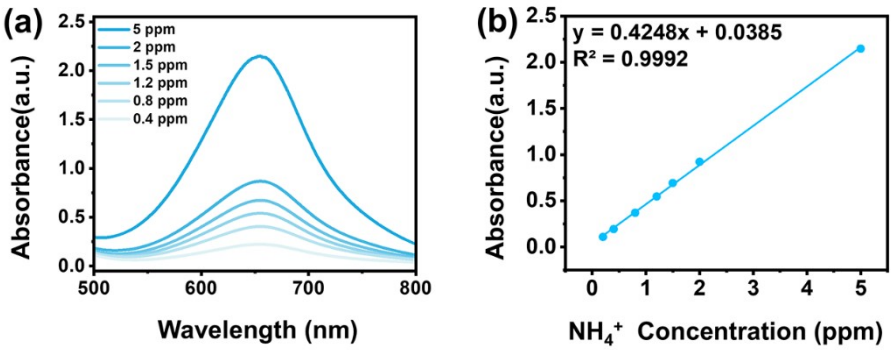

Fig. S8 (a) UV-Vis curves for different NH_4^+ concentrations. (b) Calibration curve for NH_4^+.

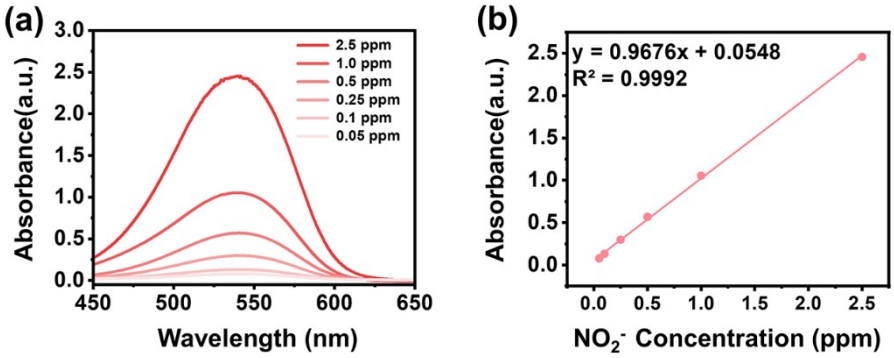

Fig. S9 (a) UV-Vis curves for different NO_2^- concentrations. (b) Calibration curve for NO_2^-.

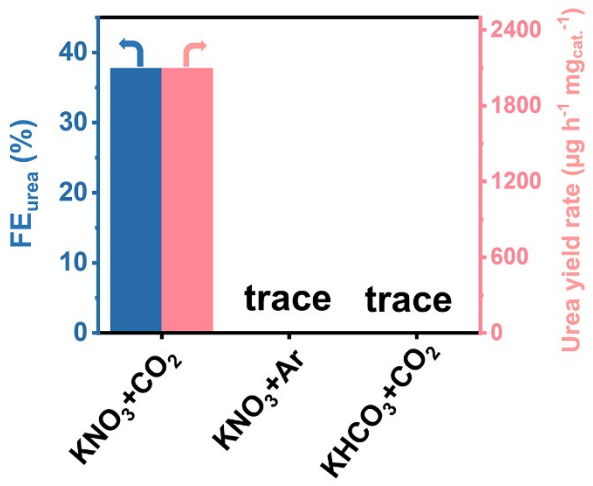

Fig. S10 Comparison of urea yield and FE under different reaction conditions.

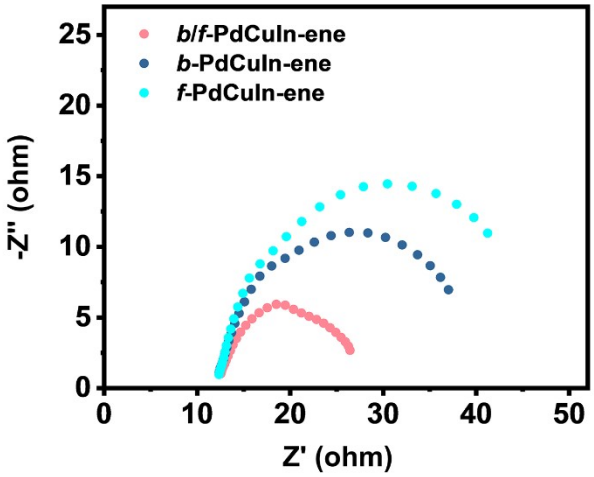

Fig. S11 EIS spectra of various catalysts.

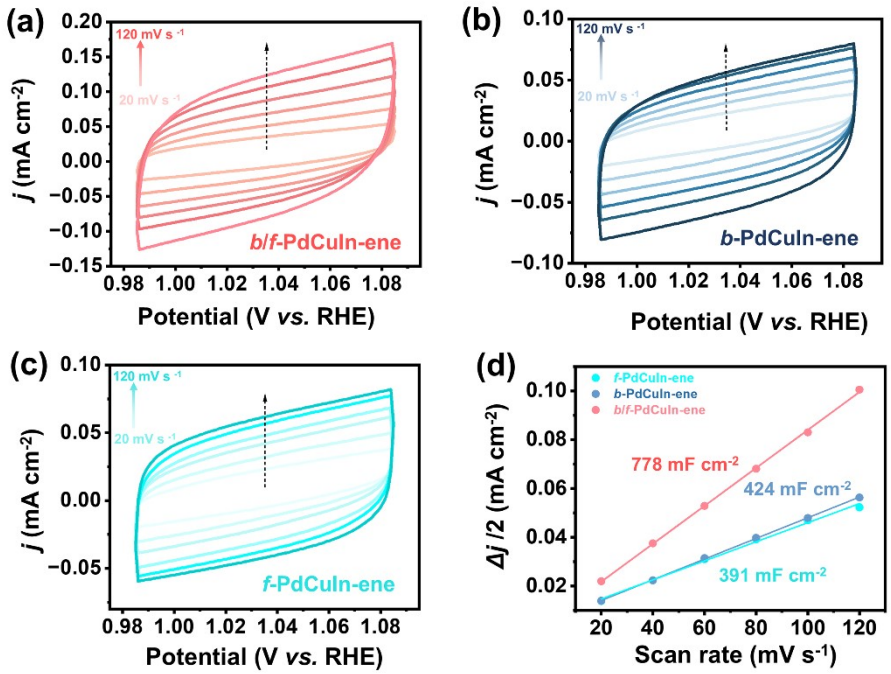

Fig. S12 CV curves at different scanning rates for (a) *b*/*f*-PdCuIn-ene, (b) *b*-PdCuIn-ene, and (c) *f*-PdCuIn-ene. (d) Charging current density differences $\Delta j/2$ plotted against scan rates and corresponding C_{dl} values for different catalysts.

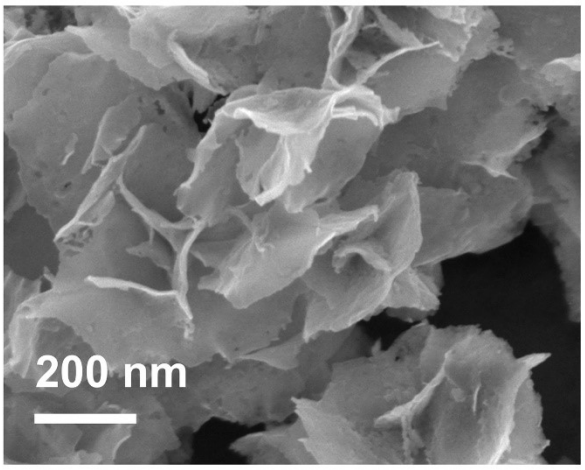

Fig. S13 SEM image of the *b*/*f*-PdCuIn-ene catalyst after stability testing.

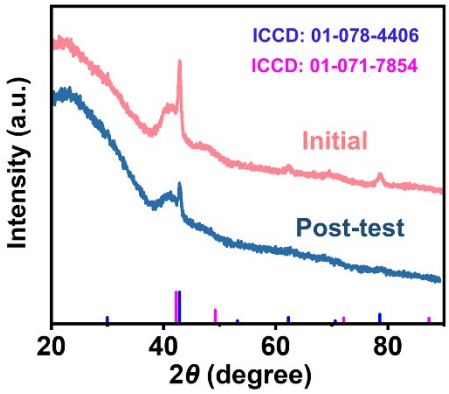

Fig. S14 XRD patterns of the *b*/*f*-PdCuIn-ene catalyst before and after stability testing.

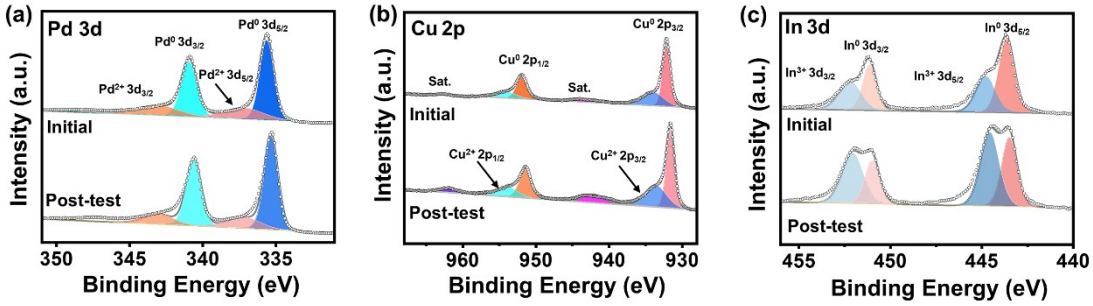

Fig. S15 XPS spectra of the *b*/*f*-PdCuIn-ene catalyst before and after stability testing.

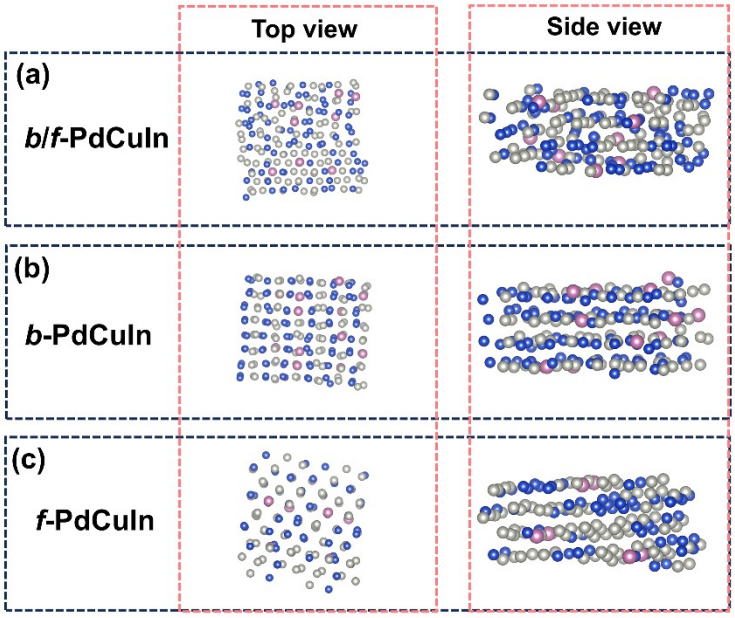

Fig. S16 Structural models of (a) *f*/*b*- PdCuIn, (b) *b*-PdCuIn, and (c) *f*-PdCuIn.

Table S1. Comparison of electrocatalytic performance of *b*/*f*-PdCuIn-ene toward urea synthesis with previously reported catalysts.

Catalysts	Reactants	Urea yield rate	FE (%)	Potential (V vs. RHE)	Ref.
***b*/*f*-PdCuIn-ene**	CO_2+KNO_3	**2096.2 μg h^{-1} $mg_{cat.}^{-1}$**	**37.7**	**-0.3**	**This work**
$PdCu/TiO_2$	CO_2+ N_2	3.36 mmol g^{-1} h^{-1} (201.8 μg h^{-1} $mg_{cat.}^{-1}$)	8.92	-0.4	[7]
VO-InOOH	CO_2+KNO_3	(592.5μg h^{-1} $mg_{cat.}^{-1}$)	51	-0.5	[8]
$BiFeO_3BiVO_4$	CO_2+N_2	4.94 mmol h^{-1} g^{-1} (296.7μg h^{-1} $mg_{cat.}^{-1}$)	17.18	-0.4	[9]
InOOH-100	CO_2+N_2	6.85 mmol h^{-1} g^{-1} (411μg h^{-1} $mg_{cat.}^{-1}$)	20.97	-0.4	[10]
Bi-BiVO4	CO_2+N_2	5.91 mmol h^{-1} g^{-1} (354.95μg h^{-1} $mg_{cat.}^{-1}$)	12.55	-0.4	[11]
AuPd	CO_2+KNO_3	204.2 μg h^{-1} $mg_{cat.}^{-1}$	15.6	-0.5	[12]
Co-PMDA-2mbIM	CO_2+N_2	14.47 mmol h^{-1} g^{-1} (868.2μg h^{-1} $mg_{cat.}^{-1}$)	48.97	-0.5	[13]
Zn foil	CO_2+NO	15.13 mmol g^{-1} h^{-1} (907.8μg h^{-1} $mg_{cat.}^{-1}$)	11.26	-0.92	[14]
F-CNT-300	CO_2+KNO_3	6.36 mmol h^{-1} g^{-1} (381.6μg h^{-1} $mg_{cat.}^{-1}$)	18	-0.65	[15]

References

1. L. Lv, H. Tan, Y. Kong, B. Tang, Q. Ji, Y. Liu, C. Wang, Z. Zhuang, H. Wang, M. Ge, M. Fan, D. Wang and W. Yan, *Angew. Chem. Int. Ed.*, 2024, **63**, e202401943.
2. G. Kresse and J. Furthmüller, *Comput. Mater. Sci.*, 1996, **6**, 15.
3. G. Kresse and J. Hafner, *Phys. Rev. B*, 1993, **47**, 558.
4. J. P. Perdew, K. Burke and M. Ernzerhof, *Phys. Rev. Lett.*, 1996, **77**, 3865.
5. V. Wang, N. Xu, J.-C. Liu, G. Tang and W.-T. Geng, *Comput. Phys. Commun.*, 2021, **267**, 108033.
6. K. Momma and F. Izumi, *J. Appl. Crystallogr.*, 2011, **44**, 1272.
7. C. Chen, X. Zhu, X. Wen, Y. Zhou, L. Zhou, H. Li, L. Tao, Q. Li, S. Du, T. Liu, D. Yan, C. Xie, Y. Zou, Y. Wang, R. Chen, J. Huo, Y. Li, J. Cheng, H. Su, X. Zhao, W. Cheng, Q. Liu, H. Lin, J. Luo, J. Chen, M. Dong, K. Cheng, C. Li and S. Wang, *Nat. Chem.,* 2020, **12**, 717.
8. C. Lv, C. Lee, L. Zhong, H. Liu, J. Liu, L. Yang, C. Yan, W. Yu, H. H. Hng, Z. Qi, L. Song, S. Li, K. P. Loh, Q. Yan and G. Yu, *ACS Nano*, 2022, **16**, 8213.
9. M. Yuan, J. Chen, Y. Bai, Z. Liu, J. Zhang, T. Zhao, Q. Shi, S. Li, X. Wang and G. Zhang, *Chem. Sci.*, 2021, **12**, 6048.
10. M. Yuan, H. Zhang, Y. Xu, R. Liu, R. Wang, T. Zhao, J. Zhang, Z. Liu, H. He, C. Yang, S. Zhang and G. Zhang, *Chem Catal.*, 2022, **2**, 309.
11. M. Yuan, J. Chen, Y. Bai, Z. Liu, J. Zhang, T. Zhao, Q. Wang, S. Li, H. He and G. Zhang, *Angew. Chem. Int. Ed.*, 2021, **60**, 10910.
12. H. Wang, Y. Jiang, S. Li, F. Gou, X. Liu, Y. Jiang, W. Luo, W. Shen, R. He and M. Li, *Appl. Catal. B: Environ.,* 2022, **318**, 121819.
13. M. Yuan, J. Chen, H. Zhang, Q. Li, L. Zhou, C. Yang, R. Liu, Z. Liu, S. Zhang and G. Zhang, *Energy Environ. Sci.,* 2022, **15**, 2084.
14. Y. Huang, R. Yang, C. Wang, N. Meng, Y. Shi, Y. Yu and B. Zhang, *ACS Energy Lett.*, 2022, **7**, 284.
15. X. Liu, P. V. Kumar, Q. Chen, L. Zhao, F. Ye, X. Ma, D. Liu, X. Chen, L. Dai and C. Hu, *Appl. Catal. B: Environ.,* 2022, **316**, 121618.